universe

MDPI

Article

GRB 181110A: Constraining the Jet Structure, Circumburst Medium and the Initial Lorentz Factor

Song Han [1,2], Xinyu Li [1,2], Luyao Jiang [1,2], Zhiping Jin [1,2], Haoning He [1,2], Yuanzhu Wang [1,2] and Daming Wei [1,2,*]

[1] Key Laboratory of Dark Matter and Space Astronomy, Purple Mountain Observatory, Chinese Academy of Sciences, Nanjing 210033, China; songhan@pmo.ac.cn (S.H.); lixy@pmo.ac.cn (X.L.); jiangly@pmo.ac.cn (L.J.); jin@pmo.ac.cn (Z.J.); hnhe@pmo.ac.cn (H.H.); wangyz@pmo.ac.cn (Y.W.)

[2] School of Astronomy and Space Science, University of Science and Technology of China, Hefei 230026, China

* Correspondence: dmwei@pmo.ac.cn

Abstract: The afterglow data of gamma ray bursts (GRBs) can be used to constrain the physical properties of the fireball (e.g., the jet structure and opening angle) and the circumburst medium. With the peak time of the early afterglow light curve being taken as the deceleration time, one can estimate the initial Lorentz factor of the fireball. In this work, we perform a comprehensive analysis on the prompt emission and the afterglow data of GRB 181110A, where a clear peak is detected by *Swift* UVOT and XRT in optical to X-ray bands. Prompt emission spectral analysis shows that the spectrum of GRB 181110A is soft, and both hard-to-soft and intensity-tracking spectral evolution are found. By fitting the afterglow light curve and building spectral energy distribution, we find that the standard external forward shock model with a constant circumburst medium is favored, and the jet structure of GRB 181110A tends to be uniform rather than structured. With the peak time of early afterglow emission, we estimate the initial fireball Lorentz factor of GRB 181110A to be $\Gamma_0 = 169^{+92}_{-40}$. We also compare GRB 181110A with other typical long GRBs in a statistical context.

Keywords: gamma-ray burst; general; radiation mechanisms; non-thermal; relativistic processes

Citation: Han, S.; Li, X.; Jiang, L.; Jin, Z.; He, H.; Wang, Y.; Wei, D. GRB 181110A: Constraining the Jet Structure, Circumburst Medium and the Initial Lorentz Factor. *Universe* **2022**, *8*, 248. https://doi.org/10.3390/universe8040248

Academic Editor: Luciano Nicastro

Received: 8 April 2022
Accepted: 15 April 2022
Published: 18 April 2022

1. Introduction

The fireball model [1–5] has long been accepted to interpret the GRB physical process. The fireball is required to move with a relativistic speed towards us to avoid the "compactness problem" [6]. The dynamical evolution of a fireball includes three phases: acceleration, coasting, and deceleration. During the acceleration phase, the Lorentz factor increases linearly with the radius r and becomes a constant after most thermal energy has been converted to kinetic [7]. After the fireball reaches the maximum Lorentz factor, it enters the "coasting" phase and moves with a constant Lorentz factor until it collects a considerable mass of ambient medium at the deceleration radius $R_{\rm dec}$, after which the Lorentz factor decays significantly. The maximum Lorentz factor during the "coasting" phase is also the initial Lorentz factor (Γ_0) of the ejecta during the deceleration phase. Panaitescu and Kumar [8] and Molinari et al. [9] have shown that $\Gamma_0 = 2\Gamma_{\rm dec}$, where $\Gamma_{\rm dec}$ is the Lorentz factor at $R_{\rm dec}$.

Γ_0 is a crucial parameter to constrain burst models [10]; however, this parameter is difficult to measure directly, unlike some other parameters, such as the isotropic energy $E_{\gamma,\rm iso}$ and the isotropic luminosity $L_{\gamma,\rm iso}$. Several methods are proposed to infer Γ_0, among which the most commonly invoked one is the afterglow onset method. The idea is that the peak time $t_{\rm p}$ of the early afterglow light curve is taken as the time when the deceleration phase begins ($t_{\rm dec}$). Given that $t_{\rm dec}$ for a constant density (ISM) medium is most sensitive to Γ but only weakly depends on other parameters, Γ_0 is possible to estimate by measuring $t_{\rm p}(t_{\rm dec})$ and $E_{\gamma,\rm iso}$ [9–12].

Before the *Swift* era, afterglow observations mostly started several hours after the burst trigger and the early optical afterglows were rarely detected. The launch of *Swift* has changed the situation. With the prompt slewing capability of the X-ray telescope (XRT [13]) and a UV-optical telescope (UVOT [14]), it enabled direct observations of the very early afterglow phase of GRBs and gained abundant early afterglow data.

In this paper, we analyze the prompt and afterglow emission of GRB 181110A, a long burst whose afterglow light curve shows a multi-band early peak.

We perform the spectral fitting for the prompt emission and calculate the peak energy E_p and $E_{\gamma,\mathrm{iso}}$. We present the optical to X-ray light curves observed by *Swift* and our fitting results. We use the temporal and spectral properties of the afterglow to infer the jet structure, the circumburst medium profile, and the initial Lorentz factor Γ_0 of GRB 181110A.

We will follow the convention $F_\nu \propto t^{-\alpha}\nu^{-\beta}$ to describe the temporal and spectral evolution of the afterglow. The concordance cosmology adopted has parameters of $H_0 = 69.6\ \mathrm{kms}^{-1}\ \mathrm{Mpc}^{-1}$, $\Omega_M = 0.286$ and $\Omega_\Lambda = 0.714$ [15]. Uncertainties are given at 68% (1σ) confidence level for one parameter unless stated otherwise.

2. Observations and Data

GRB 181110A was detected by *Swift* at 08:43:31 UT on 10 November 2018 [16]. The BAT light curve showed a multi-peaked structure with a duration of $T_{90} = 138.4 \pm 10.9$ s [17]. The *Swift* XRT began observing the field 64 s after the BAT trigger. A bright, uncatalogued X-ray source was located with an enhanced position of RA (J2000): 20 h 09 m 16.32 s and Dec (J2000): -36d 53′ 47.9″ with an uncertainty of 1.4 arcsec (at 90% confidence level) [18]. The *Swift* UVOT began settled observations of the field of GRB 181110A 72 s after the BAT trigger [19]. In the initial exposures, UVOT detected an optical counterpart consistent with the XRT position (Figure 1). The redshift of GRB 181110A is z = 1.505 [20].

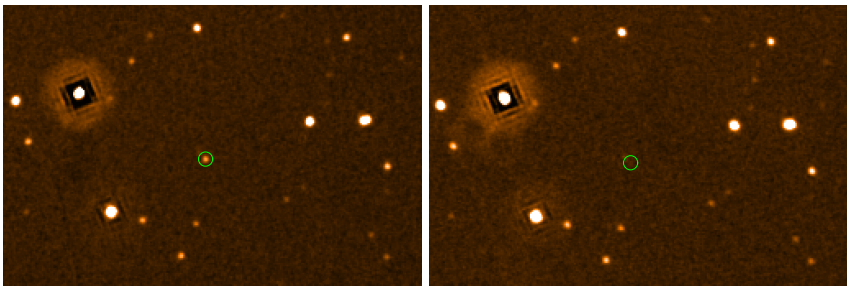

Figure 1. *Swift* UVOT B-band images of the field of GRB 181110A about 2 (**left**) and 14 (**right**) hours after the trigger; the optical afterglow is circled out.

The light curve and spectral data of BAT[1] and XRT were obtained from the *Swift* online repository[2] on 9 November 2021. The BAT data we selected (15 keV to 150 keV) are analyzed with the HEASOFT package (version 6.28) and Xspec 12.11.1[3].

3. Analysis

3.1. Afterglow Light Curve Modeling

Figure 2 shows the optical, ultraviolet, and X-ray light curves of the afterglow of GRB 181110A. The data were taken with *Swift* XRT and UVOT. The light curves of different energy bands evolve nearly synchronously and show a peak around 1200 s.

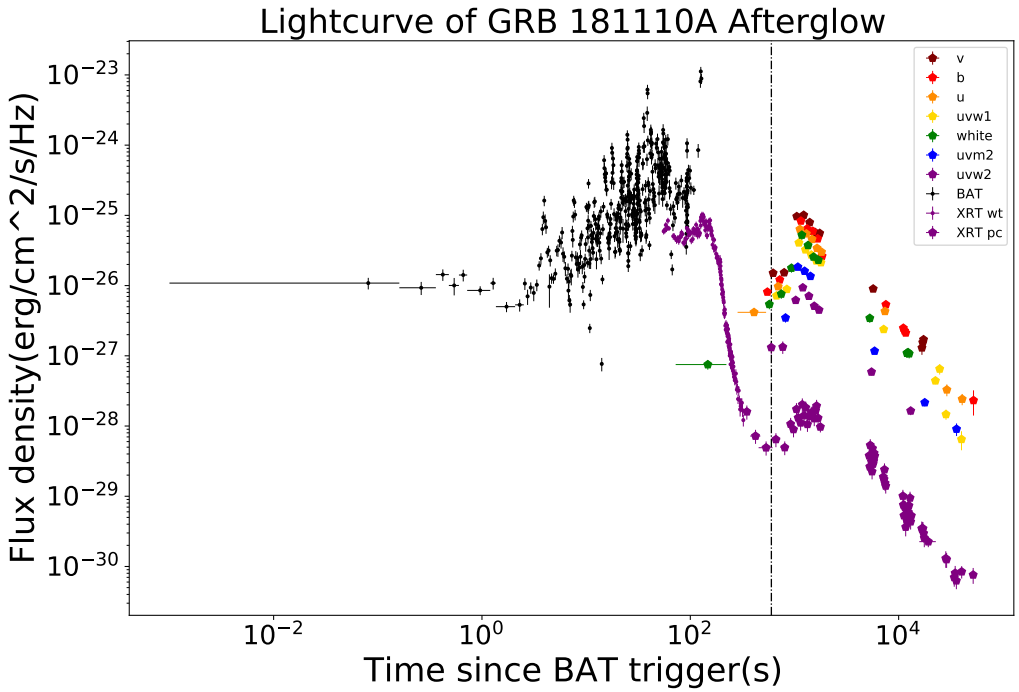

Figure 2. The optical, ultraviolet, and X-ray light curves of GRB 181110A. The UVOT data have been corrected for Galactic extinction. The dashed line marks the time $t = 600$ s.

To derive the peak time and slopes of rise and decay phase, we use a smoothly broken power-law function to fit the light curves [21]:

$$F(t) = F_0 \left[\left(\frac{t}{t_b} \right)^{\kappa\alpha_1} + \left(\frac{t}{t_b} \right)^{\kappa\alpha_2} \right]^{-1/\kappa}, \kappa > 0 \quad (1)$$

where t is the time after the trigger, F_0 is the normalization constant, κ is the smoothness parameter, and α_i is the slope of rise or decay phase ($\alpha_1 < 0, \alpha_2 > 0$). Following [9,22], the light curve reaches the maximum at

$$t_p = t_b(-\alpha_1/\alpha_2)^{1/\kappa(\alpha_2-\alpha_1)} \quad (2)$$

We choose the data from 600 s after the trigger to fit since as shown in Figure 2, the earlier part may be affected by the prompt emission.

We set $F_0, t_b, \alpha_i, \kappa$ as free parameters and use `emcee` [23], the Python ensemble sampling toolkit for affine-invariant MCMC to fit the observed data with Equation (1). We first fit the data of different bands separately and the results are quite similar; thus, we fit them with a unified model. The peak time (t_p) of optical and UV light curves is about 1200 s. The best-fitting results are listed in Table 1 and the corresponding curves are shown in Figure 3.

Table 1. Best-fit values of multiband afterglow of GRB 181110A.

t_p(s)	t_b(s)	α_1	α_2	κ
1193^{+12}_{-11}	1179^{+12}_{-11}	$-3.15^{+0.12}_{-0.12}$	$1.55^{+0.01}_{-0.01}$	$12.81^{+1.56}_{-2.36}$

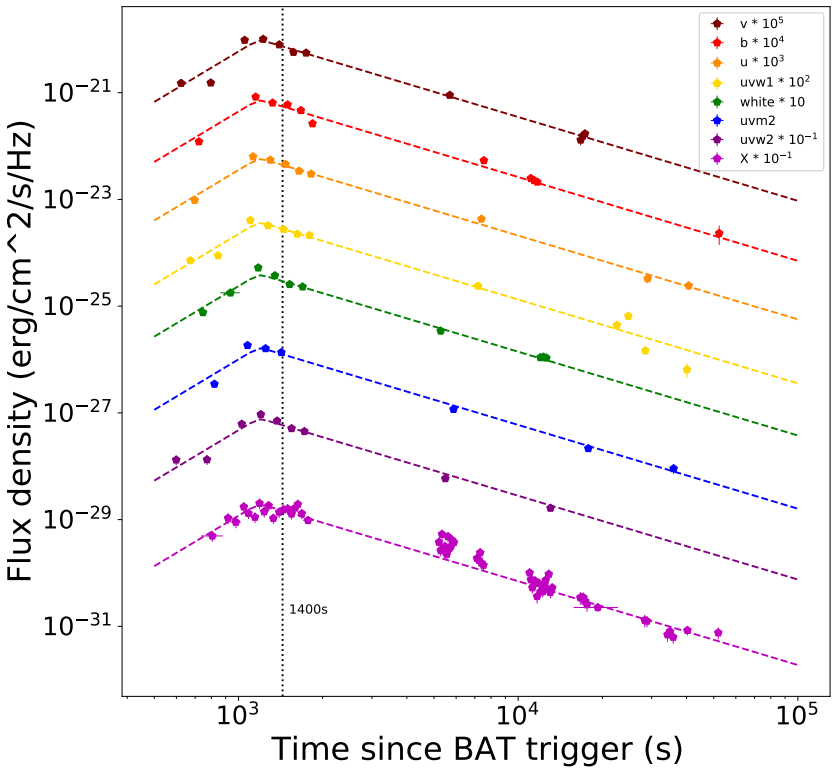

Figure 3. The light curves of GRB 181110A. The best-fitting results using the smoothly broken power-law model are shown as dashed lines. The black vertical line marks the time (1400 s) where we build spectral energy distribution.

3.2. Spectral Analysis

3.2.1. Prompt Emission Spectral Analysis

We perform both time-integrated and time-resolved spectral analyses within the T_{90} time interval from $T_0 - 39.21$ s to $T_0 + 99.16$ s. The time-resolved spectral analysis is performed by slicing the T_{90} interval into time bins with the Bayesian block [24]. The cutoff power-law function (CPL) and the single power-law (PL) function are adopted to fit the data. The CPL function is described as

$$N(E) = A(\frac{E}{100\ \mathrm{keV}})^{\alpha}\exp(-\frac{E}{E_c}) \tag{3}$$

where A is the normalization coefficient, α is the low-energy photon spectral index, and E_c is the break energy of the photon spectrum, and it is related to the peak energy (E_p) of the $E^2N(E)$ spectrum by $E_p = (2+\alpha)E_c$. The single power-law (PL) function is

$$N(E) = A \cdot E^{\alpha_1} \tag{4}$$

where A is the normalization coefficient and α_1 is the single power-law photon index.

The time-integrated BAT spectrum ($T_0 - 39.21$ s to $T_0 + 99.16$ s) is well fitted by CPL function ($\chi^2/\mathrm{dof} = 0.96$), with a photon index $\alpha = -1.76 \pm 0.12$ and $E_p = 52.87 \pm 37.28$ keV. We calculate the isotropic energy $E_{\gamma,\mathrm{iso}} = (13.43 \pm 3.49) \times 10^{52}$ erg.

For the time-resolved spectrum, we first fit the spectrum using the CPL function. Given the narrow energy band of BAT, we use the PL function to fit for the time bins in which E_p cannot be reliably constrained. Our result indicates the temporal evolution of the spectra, which is shown in Table 2. The energy spectrum index of GRB 181110A is found to be soft on the whole, and the spectral evolution is observed, as shown in Figure 4; α shows a hard-to-soft pattern at first and then shows an intensity-tracking pattern.

Table 2. Results for the time-resolved spectral analysis (15 keV∼150 keV).

Time Interval	CPL		PL		
(s)	α	E_p (keV)	α_1	Flux $\times 10^{-8}$(erg/cm^2/s)	Red.χ^2
−39.21∼−8.71	...	...	-1.33 ± 0.10	3.02 ± 0.45	1.08
−8.71∼2.28	...	...	-1.70 ± 0.07	7.32 ± 0.63	0.87
2.28∼9.28	-1.06 ± 0.24	80.02 ± 38.25	...	12.17 ± 7.29	0.83
9.28∼10.28	-0.76 ± 0.47	74.39 ± 51.74	...	15.85 ± 12.62	1.07
10.28∼13.28	-1.37 ± 0.25	111.61 ± 102.43	...	18.42 ± 17.30	1.09
13.28∼20.28	-1.55 ± 0.24	58.70 ± 48.94	...	11.43 ± 7.61	1.07
20.28∼23.38	-1.36 ± 0.36	42.03 ± 32.97	...	11.95 ± 10.62	0.83
23.38∼26.28	-1.50 ± 0.26	73.83 ± 67.34	...	16.80 ± 16.28	0.75
26.28∼29.58	...	...	-1.99 ± 0.09	11.05 ± 1.21	0.73
29.58∼32.06	-1.64 ± 0.26	58.26 ± 61.75	...	18.81 ± 16.95	0.58
32.06∼42.64	-1.77 ± 0.30	20.71 ± 29.25	...	7.67 ± 5.92	1.04
42.64∼52.19	...	...	-2.53 ± 0.11	4.90 ± 0.77	0.79
52.19∼54.36	...	...	-2.24 ± 0.12	9.35 ± 1.95	0.96
54.36∼59.76	...	...	-2.33 ± 0.10	7.91 ± 1.00	1.05
59.76∼69.06	...	...	-2.08 ± 0.11	4.75 ± 0.72	1.09
69.06∼89.76	...	...	-2.29 ± 0.14	2.39 ± 0.54	1.04
89.76∼91.53	...	...	-2.39 ± 0.19	5.27 ± 2.61	0.86
91.53∼94.31	-0.61 ± 0.61	26.30 ± 14.56	...	8.45 ± 7.43	0.95
94.31∼99.16	...	...	-2.80 ± 0.27	2.55 ± 1.74	1.28

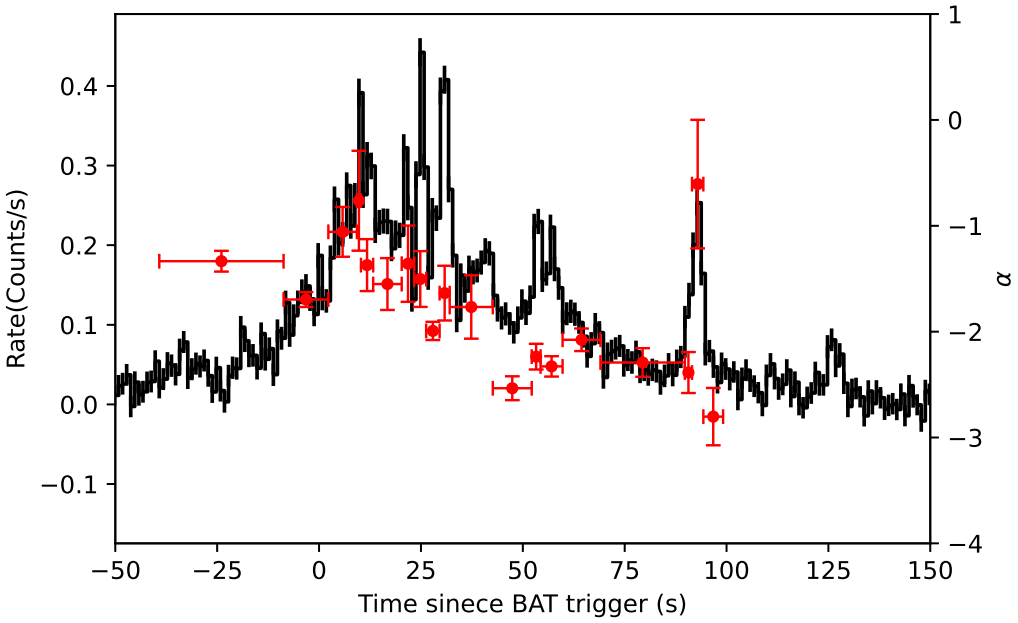

Figure 4. The spectral evolution feature of GRB 181110A. Red markers refer to the spectral index α. A hard-to-soft spectral index evolution is present in the initial part of the burst, followed by an intensity-tracking pattern.The red points indicate the spectral index α and α shows a hard-to-soft pattern at first and then an intensity-tracking pattern.

3.2.2. Afterglow SED Fitting

In Figure 5, we build the spectral energy distribution (SED) at 1400 s after the trigger. This epoch is chosen because multiband data are available. The SED has been corrected for extinction in the Milky Way ($E(B-V) = 0.0613$ [25]) and X-ray absorption ($N_H = 5.51 \times 10^{15}\,\mathrm{cm}^{-2}$ [26]). In addition, to account for host galaxy dust extinction, we fit the afterglow SED with the Small Magellan Cloud (SMC) template extinction law [27–29] and derive a small visual extinction ($A_\mathrm{v} = 0.09^{+0.01}_{-0.01} A_\mathrm{v} = 0.09$), taking the Lyman alpha absorption at $z = 1.505$ into account. Overall, the SED is consistent with a simple power-law

extending from optical to X-ray band and the spectral slope is $\beta = 0.99^{+0.02}_{-0.03}$, which is in line with the average spectral index for XRT PC mode data ($\beta_X = 0.82^{+0.27}_{-0.20}$) retrieved from the online repository[4].

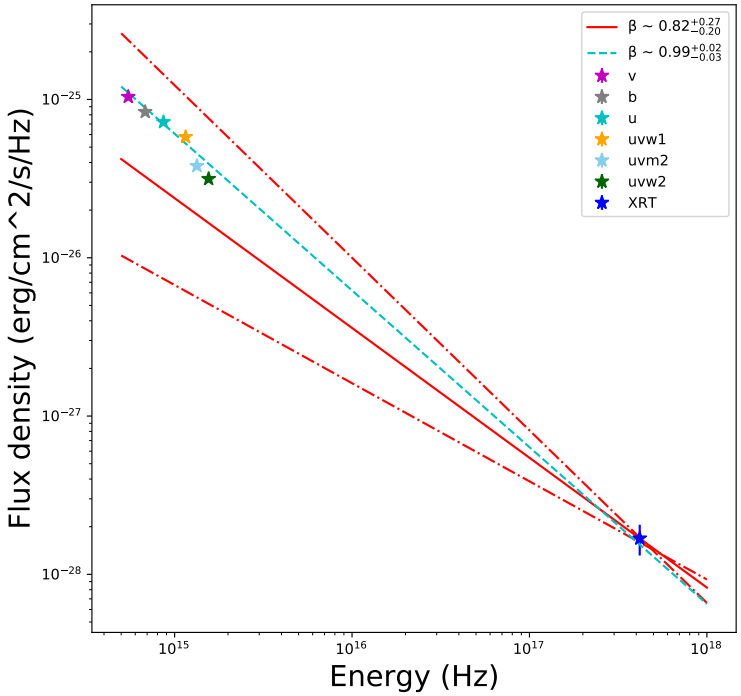

Figure 5. Optical to X-ray SED of GRB 181110A at 1400 s after BAT trigger. The data have been corrected for galactic and host extinction and X-ray absorption. Note that the flux drops at the uvm2 and uvw2 bands because of the Lyman alpha absorption. The SED is well fitted with a single power-law (cyan line). The red lines indicate the spectrum and its uncertainties derived from the time-averaged PC mode data [30].

3.3. `Afterglowpy` Modeling

To further investigate the properties of the relativistic jet, we numerically model the afterglow light curves (from 5000 s after the trigger) using `afterglowpy` [31]. Three structures for the jet's energy profile are considered: the top-hat, the Gaussian, and the power-law jets [32–36]. The physical parameters for the top-hat model are the viewing angle (θ_v), the jet core opening angle (θ_c), the isotropic energy ($E_{K,iso}$), the circumburst medium density (n_0), and the fraction of shock energy that is transferred to electron and the magnetic field, respectively (ϵ_e and ϵ_B). The Gaussian and power-law models have the truncation angle (θ_w) as an additional free parameter, and the power-law model has the power-law index (b) as another additional parameter. Then, with `emcee`, we show the results of physical parameters in Table 3. The posterior distribution of physical parameters of top-hat jet for GRB 181110A is presented in Figure 6.

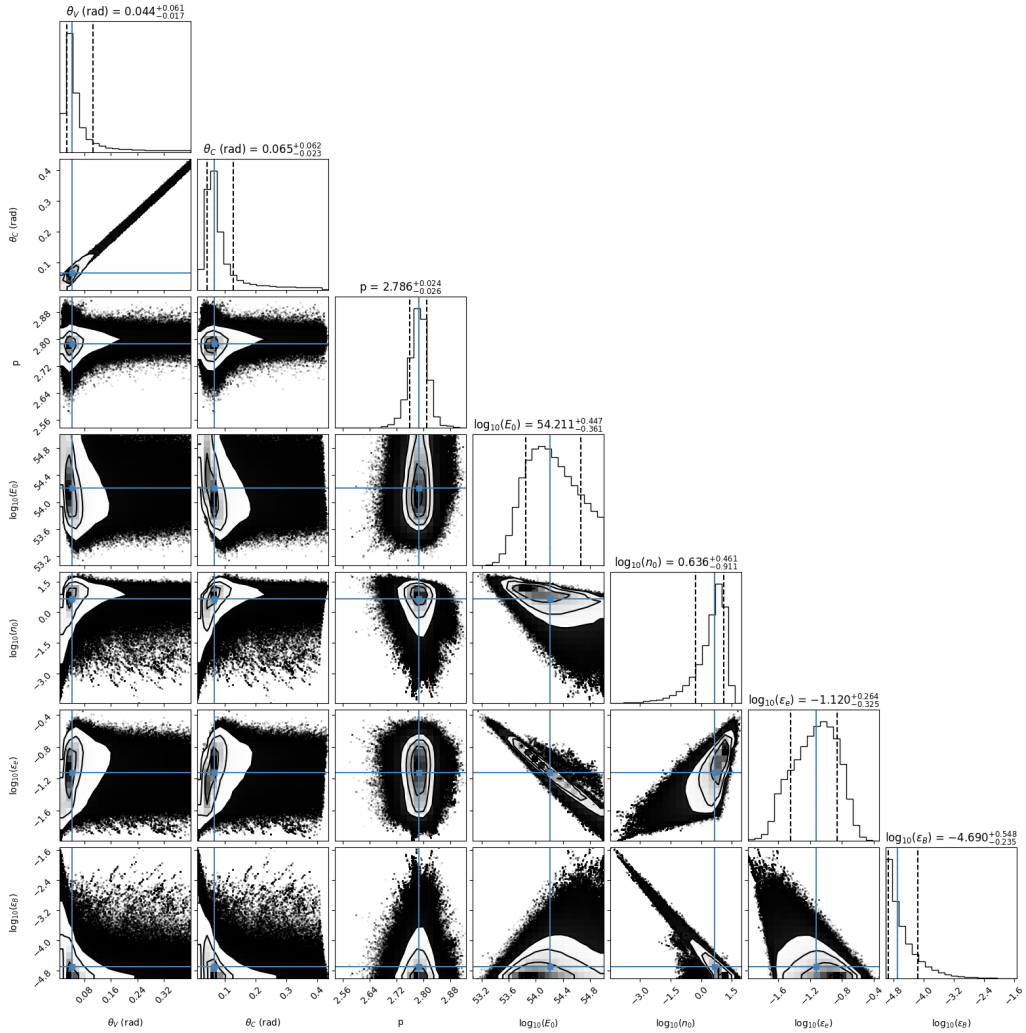

Figure 6. The posterior distribution of physical parameters of top-hat jet for GRB 181110A. Dashed lines mark the 1σ region.

Table 3. Physical parameters for GRB 181110 A.

	Top-Hat	**Gaussian**	**Power-Law**
$\theta_{\rm v}$[rad]	$0.044^{+0.061}_{-0.017}$	$0.083^{+0.192}_{-0.049}$	$0.011^{+0.010}_{-0.007}$
$\log_{10} E_0$	$54.211^{+0.447}_{-0.361}$	$54.174^{+0.432}_{-0.336}$	$53.878^{+0.409}_{-0.310}$
$\theta_{\rm c}$[rad]	$0.065^{+0.062}_{-0.023}$	$0.332^{+0.494}_{-0.167}$	$0.014^{+0.006}_{-0.003}$
$\theta_{\rm w}$[rad]		$0.106^{+0.191}_{-0.050}$	$0.856^{+0.491}_{-0.493}$
b			$0.858^{+0.356}_{-0.284}$
p	$2.786^{+0.024}_{-0.026}$	$2.792^{+0.023}_{-0.026}$	$2.493^{+0.165}_{-0.168}$
$\log_{10} n_0$	$0.636^{+0.461}_{-0.911}$	$0.745^{+0.388}_{-0.711}$	$1.640^{+0.677}_{-0.709}$
$\log_{10} \epsilon_{\rm e}$	$-1.120^{+0.264}_{-0.325}$	$-1.078^{+0.240}_{-0.310}$	$-0.718^{+0.277}_{-0.361}$
$\log_{10} \epsilon_B$	$-4.690^{+0.548}_{-0.235}$	$-4.750^{+0.430}_{-0.188}$	$-4.685^{+0.458}_{-0.232}$

4. Discussion

4.1. Constraint on the Medium Profile and Jet Structure

In the standard afterglow model, the interaction between the relativistic fireball and the circumburst medium leads to external shocks and produces the multiband afterglow emission. The temporal and spectral behavior of multiband afterglow can be used to diagnose the profile of the circumburst medium. For GRB 181110A, we firstly consider the ISM case. When $t < t_{\rm p}$, the fireball has not been decelerated significantly, and the flux of the forward shock emission can be described by the scaling law [37]:

$$F_\nu = F_{\nu,\max}(\nu/\nu_m)^{-(p-1)/2} \propto t^3\nu^{-(p-1)/2} \tag{5}$$

for $\nu_m < \nu < \nu_c$, where ν_m and ν_c are the typical synchrotron frequency and the cooling frequency of electrons, respectively. The best-fitting parameters listed in Table 1 are therefore consistent with the temporal behavior above. When $t > t_{\rm p}$, the temporal decay index ($\alpha = 1.55^{+0.01}_{-0.01}$) in Table 1 and the spectral index ($\beta = 0.99^{+0.02}_{-0.03}$) derived from our analysis are consistent with the closure relation $\alpha = 3\beta/2$ in $\nu_m < \nu < \nu_c$ case [37]. The electron energy spectral index is estimated to be $p \sim 3$ with the relation $\beta = (p-1)/2$, while in the wind scenario, the rise of the forward shock emission for $t < t_{\rm p}$ cannot be steeper than $t^{1/2}$ [38]. Hence, a homogeneous medium model is favored for GRB 181110A.

Note that the electron energy spectral index $p \sim 3$ is closer to the results of top-hat and Gaussian jet in Table 3. In addition, for the Gaussian model, the constrained jet profile is similar to that of the top-hat model due to $\theta_w < \theta_c$ [31]. The similar results between these two models in Table 3 also favor a uniform jet over a structured one.

Using the parameters in Table 3, we further estimate the typical frequencies of electrons and find $\nu_m \sim 10^{12}$ Hz and $\nu_c \sim 10^{19}$ Hz, which is consistent with our analysis above ($\nu_m < \nu < \nu_c$).

4.2. Determination of Γ_0

According to the fits, the early afterglow peaks at about 1193 s after the trigger, thus $t_{\rm p} > T_{90}$, which agrees with the ISM "thin shell" case [39]. In the thin shell case, the fireball decelerates at $t_{\rm dec} = t_\gamma$, where t_γ is the timescale over which the ISM mass collected by fireball is $1/\gamma_{\rm dec}$ of the ejecta mass, i.e.,

$$t_{\rm dec} \equiv t_\gamma \sim \frac{R_{\rm dec}}{2c\gamma_{\rm dec}^2} = \left(\frac{3E_{\gamma,\rm iso}}{32\pi\gamma_{\rm dec}^8\eta n_0 m_{\rm p}c^5}\right)^{1/3} \tag{6}$$

where $\eta = E_{\gamma,\rm iso}/E_{K,\rm iso}$ is the ratio between the isotropic gamma-ray energy and the isotropic blast wave kinetic energy, n_0 is the particle number density, $m_{\rm p}$ is the proton mass, and $\gamma_{\rm dec}$ is the fireball Lorentz factor at $t_{\rm dec}$, which is approximately half of Γ_0 [40]. Therefore, we can estimate Γ_0 by

$$\Gamma_0 = 2\left[\frac{3E_{\gamma,\rm iso}(1+z)^3}{32\pi n_0 m_{\rm p}c^5\eta t_{\rm p}^3}\right]^{1/8} \approx 235\left[\frac{E_{\gamma,\rm iso,52}(1+z)^3}{\eta_{0.2}n_0 t_{\rm p,2}^3}\right]^{1/8} \tag{7}$$

The notation Q_n denotes $Q/10^n$ in cgs for $E_{\gamma,\rm iso}$ and $t_{\rm p}$, $\eta_{0.2} = \eta/0.2$. With the parameters obtained in the previous section, we can obtain $n_0 = 4.33^{+8.18}_{-3.79}\,{\rm cm}^{-3}$, $\eta \approx 0.08^{+0.16}_{-0.06}$, and then we derive $\Gamma_0 = 169^{+92}_{-40}$.

The value of Γ_0 confirms the highly relativistic nature of GRB fireballs and is within the typical range ($100 \lesssim \Gamma_0 \lesssim 1000$) (see Figure 11 in [41]). With Γ_0, we can also derive the deceleration radius $R_{\rm dec} \approx 2t_{\rm p}c\gamma_{\rm dec}^2/(1+z) \approx 2.3 \times 10^{17}$ cm.

4.3. GRB 181110A in a Statistical Context

By analyzing a sample of GRBs with afterglow onset feature, Liang et al. [12,42,43] found strong correlations among the timescales of the onset "bump" and correlations among $E_{p,z}$, Γ_0 and $E_{\gamma,\rm iso}$, where $E_{p,z} = E_p(1+z)$ is the peak energy in the cosmological rest frame. Following [12], we take the full width at half-maximum (FWHM) of our fitting light curve as the characteristic width (w) of the peak. The rising and decaying timescales (t_r and t_d) are measured at FWHM. Their correlations are as follows [12,42]:

$$\log t_{\rm d} = (0.48 \pm 0.13) + (1.06 \pm 0.06) \log t_{\rm r} \quad (8)$$

$$\log w = (0.17 \pm 0.20) + (1.06 \pm 0.08) \log t_{\rm p} \quad (9)$$

We examine whether GRB 181110A satisfies these empirical relations and then we compare GRB 181110A with other bursts in the Amati relation [44–46]:

$$E_{\rm p}/(1+z) = (3.24 \pm 0.07) + (0.54 \pm 0.04) \log(E_{\gamma,\rm iso}/10^{52}\,{\rm erg}) \quad \text{for SGRBs} \quad (10)$$

and

$$E_{\rm p}/(1+z) = (2.22 \pm 0.03) + (0.47 \pm 0.03) \log(E_{\gamma,\rm iso}/10^{52}\,{\rm erg}) \quad \text{for LGRBs} \quad (11)$$

As shown in Figures 7 and 8, the $E_{\gamma,\rm iso}$ and $E_{p,z}$ of this burst lie within the LGRB distribution of Amati relation. The correlations among the timescales of the onset "bump" suggest that a wider onset "bump" tends to peak at a later time, which is consistent with t_p and w we derived for GRB 181110A. GRB 181110A also shares the same $\Gamma_0 - E_{p,z}$ and $\Gamma_0 - E_{\gamma,\rm iso}$ empirical relations with other typical GRBs, which read [43]:

$$\log(E_{\rm p,z}/{\rm keV}) = (0.77 \pm 0.40) + (0.82 \pm 0.18) \log \Gamma_0 \quad (12)$$

$$\log E_{\gamma,\rm iso,52} = -(3.06 \pm 0.59) + (1.78 \pm 0.26) \log \Gamma_0 \quad (13)$$

These consistencies suggest that GRB 181110A belongs to typical long GRBs with an afterglow onset feature which can be interpreted by a standard external forward shock model.

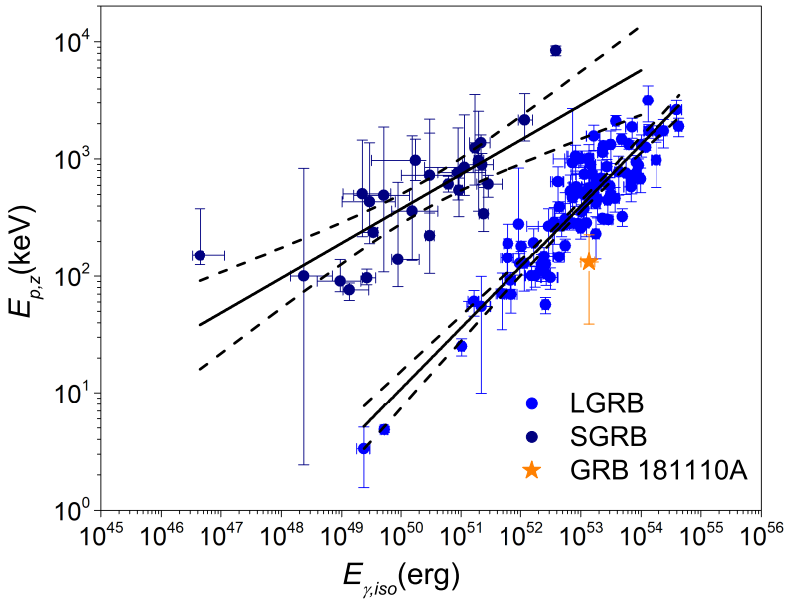

Figure 7. GRB 181110A (orange) in Amati relation. The solid lines are the best fits: $\log E_{\rm p}/(1+z) = (3.24 \pm 0.07) + (0.54 \pm 0.04) \log(E_{\gamma,\rm iso}/10^{52}\,{\rm erg})$ for SGRBs, and $\log E_{\rm p}/(1+z) = (2.22 \pm 0.03) + (0.47 \pm 0.03) \log(E_{\gamma,\rm iso}/10^{52}\,{\rm erg})$for LGRBs and SGRBs, respectively (data from [46]). The dashed lines mark the 2σ region of the correlation.

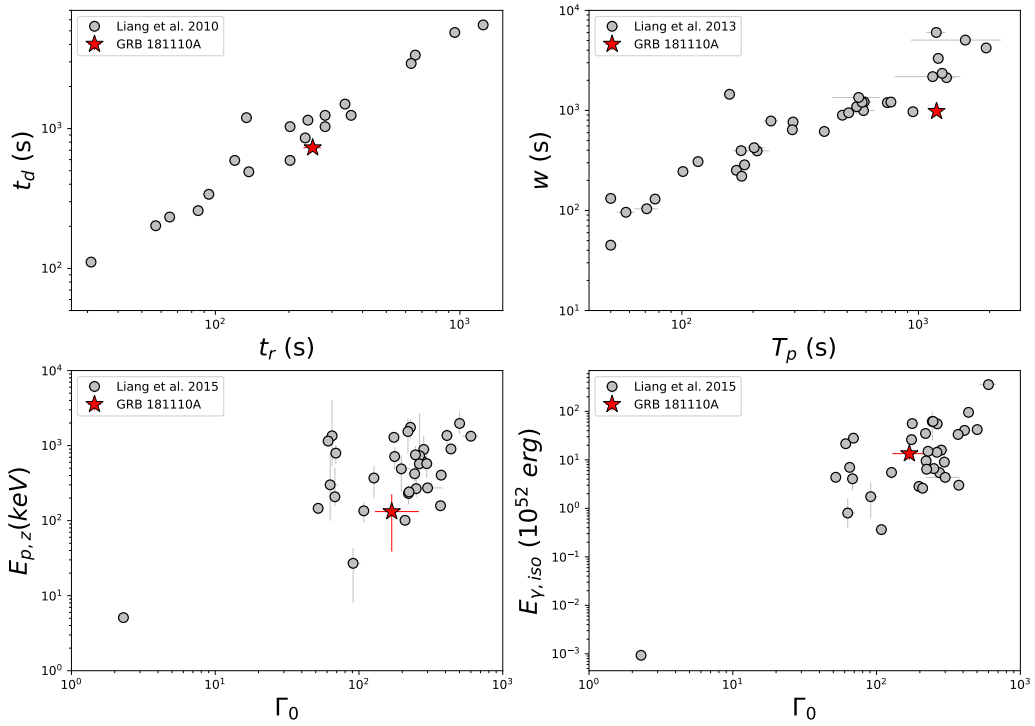

Figure 8. Correlations among timescales of GRB afterglow onset "bump" and the $E_{p,z} - \Gamma_0$, $E_{\gamma,\mathrm{iso}} - \Gamma_0$ correlation (8), (12). GRB 181110A (marked with a red star) locates within the sample of GRBs with the onset feature (marked with silver circles; data from [12,42,43]).

5. Summary

The early afterglow light curve of GRB 181110A shows a peak at about 1200 s, thus it is possible to estimate the fireball initial Lorentz factor by taking the peak time t_p as deceleration time t_{dec}.

Firstly we perform spectral analyses for the prompt emission of GRB 181110A and the time-integrated BAT spectrum ($T_0 - 39.21$ s to $T_0 + 99.16$ s) is well fitted by the CPL function with $\alpha = -1.76 \pm 0.12$ and $E_{\mathrm{p}} = 52.87 \pm 37.28$ keV, while we fit the time-resolved spectrum with both CPL and PL function. We derive $E_{\gamma,\mathrm{iso}} = (13.43 \pm 3.49) \times 10^{52}$ erg. We also find that GRB 181110A has a soft spectrum and a spectral evolution feature; the evolution shows a hard-to-soft pattern at first and then an intensity-tracking pattern.

We fit the afterglow light curves with a smoothly broken power-law model and find that the light curves of all bands show the same temporal behavior. For GRB 181110A, the sharp rise of the very early afterglow light curve has ruled out a wind-like circumburst medium. Our joint analysis of multiband afterglow indicates that the standard external forward shock model with the ISM scenario is favored, and the cooling frequency ν_c is likely above X-ray band.

We also use `afterglowpy` to model the afterglow light curves numerically and find that the jet of GRB 181110A tends to be uniform rather than structured.

We investigate GRB 181110A in a statistical context and find that it locates within the sample of LGRBs with good afterglow onset features. The $E_{\gamma,\mathrm{iso}}$ and $E_{p,z}$ we derived agree with the Amati relation for LGRBs. With the peak time of light curve t_{p} and parameters given by `afterglowpy` modeling, the initial Lorentz factor is measured to be $\Gamma_0 \sim 169$, which is consistent with the typical values of GRBs ($100 \lesssim \Gamma_0 \lesssim 1000$). Overall, for those GRBs with multiband data observed, it is possible to infer the structures of their jets. GRB 181110A is a typical long GRB that shows a clear afterglow onset feature; with more GRBs such as this being detected, our knowledge of the GRB fireball and circumburst environment may be extended.

Author Contributions: Conceptualization, D.W. and Z.J.; methodology, S.H., X.L. and L.J.; software, S.H., X.L. and L.J.; formal analysis, S.H.; investigation, S.H.; data curation, S.H. and L.J.; writing—original draft preparation, S.H.; writing—review and editing, S.H., Y.W. and D.W.; visualization, S.H., X.L. and L.J.; supervision, D.W.; project administration, D.W., Z.J. and H.H.; funding acquisition, D.W. All authors have read and agreed to the published version of the manuscript.

Funding: This work was supported by NSFC (No. 12073080, 11933010, 11921003) and by the Chinese Academy of Sciences via the Key Research Program of Frontier Sciences (No. QYZDJ-SSW-SYS024).

Data Availability Statement: This work made use of data supplied by the UK Swift Science Data Centre at the University of Leicester (https://www.swift.ac.uk/burst_analyser/00871316/) on 9 November 2021. The BAT data are analysed with the HEASOFT package and Xspec (https://heasarc.gsfc.nasa.gov/xanadu/xspec (accessed on 8 April 2022)).

Conflicts of Interest: The authors declare no conflict of interest.

Notes

[1] https://heasarc.gsfc.nasa.gov/cgi-bin/W3Browse/swift.pl (accessed on 8 April 2022)
[2] https://www.swift.ac.uk/burst_analyser/00871316/ (accessed on 8 April 2022)
[3] https://heasarc.gsfc.nasa.gov/xanadu/xspec (accessed on 8 April 2022)
[4] https://www.swift.ac.uk/burst_analyser/00871316/(accessed on 8 April 2022)

References

1. Rees, M.J.; Mészáros, P. Relativistic fireballs—Energy conversion and time-scales. *Mon. Not. R. Astron. Soc.* **2007**, *258*, 41–43. [CrossRef]
2. Mészáros, P.; Rees, M.J. Relativistic Fireballs and Their Impact on External Matter: Models for Cosmological Gamma-Ray Bursts. *Astrophys. J.* **1993**, *405*, 278–284. [CrossRef]
3. Piran, T. Gamma-ray bursts and the fireball model. *Phys. Rep.* **1999**, *314*, 575–667. [CrossRef]
4. Mészáros, P. Theories of Gamma-Ray Bursts. *Annu. Rev. Astron. Astrophys.* **2002**, *314*, 137–169. [CrossRef]
5. Zhang, B.; Mészáros, P. Gamma-Ray Bursts: Progress, problems & prospects. *Int. J. Mod. Phys.* **2004**, *19*, 2385–2472.
6. Ruderman, M. Theories of gamma-ray bursts. In Proceedings of the Seventh Texas Symposium on Relativistic Astrophysics, Dallas, TX, USA, 16–20 December 1974.
7. Piran, T.; Shemi, A.; Narayan, R. Hydrodynamics of Relativistic Fireballs. *Mon. Not. R. Astron. Soc.* **1993**, *263*, 861–867. [CrossRef]
8. Panaitescu, A.; Kumar, P. Analytic Light Curves of Gamma-Ray Burst Afterglows: Homogeneous versus Wind External Media. *Astrophys. J.* **2000**, *543*, 66–76. [CrossRef]
9. Molinari, E.; Vergani, S.D.; Malesani, D.; Covino, S.; d'Avanzo, P.; Chincarini, G.; Zerbi, F.M.; Antonelli, L.A.; Conconi, P.; Testa, V.; et al. REM observations of GRB 060418 and GRB 060607A: The onset of the afterglow and the initial fireball Lorentz factor determination. *Astron. Astrophys.* **2007**, *469*, L13–L16. [CrossRef]
10. Sari, R.; Piran, T. Predictions for the Very Early Afterglow and the Optical Flash. *Astrophys. J.* **1999**, *520*, 641–649. [CrossRef]
11. Xue, R.R.; Fan, Y.Z.; Wei, D.M. The initial Lorentz factors of fireballs inferred from the early X-ray data of SWIFT GRBs. *Astron. Astrophys.* **2009**, *498*, 671–676. [CrossRef]
12. Liang, E.W.; Yi, S.X.; Zhang, J. Constraining Gamma-ray Burst Initial Lorentz Factor with the Afterglow Onset Feature and Discovery of a Tight Γ_0-E $_{\gamma,iso}$ Correlation. *Astrophys. J.* **2010**, *725*, 2209–2224. [CrossRef]
13. Burrows, D.N.; Hill, J.E.; Nousek, J.A.; Kennea, J.; Wells, A.; Osborne, J.P.; Abbey, A.F.; Beardmore, A.; Mukerjee, K.; Short, A.D.T.; et al. The Swift X-Ray Telescope. *Space Sci. Rev.* **2005**, *120*, 165–195. [CrossRef]
14. Roming, P.W.A.; Kennedy, T.E.; Mason, K.O.; Nousek, J.A.; Ahr, L.; Bingham, R.E.; Broos, P.S.; Carter, M.J.; Hancock, B.K.; Huckle, H.E.; et al. The Swift Ultra-Violet/Optical Telescope. *Space Sci. Rev.* **2005**, *120*, 95–142. [CrossRef]
15. Bennett, C.L.; Larson, D.R.; Weiland, J.L.; Hinshaw, G. The 1% Concordance Hubble Constant. *Astrophys. J.* **2014**, *794*, 135. [CrossRef]
16. Evans, P.A.; Page, K.L.; Sakamoto, T. *GRB 181110A: Swift Detection of a Burst with an Optical Counterpart*; GRB Coordinates Network, Circular Service, No. 23413, #1; NASA: Washington, DC, USA, 2018.
17. Lien, A.Y.; Barthelmy, S.D.; Cummings, J.R.; Evans, P.A.; Krimm, H.A.; Markwardt, C.B.; Palmer, D.M.; Sakamoto, T.; Stamatikos, M.; Ukwatta, T.N. *GRB 181110A, Swift-BAT Refined Analysis*; GRB Coordinates Network, Circular Service, No. 23420, #1; NASA: Washington, DC, USA, 2018.
18. Goad, M.R.; Osborne, J.P.; Beardmore, A.P.; Evans, P.A. *GRB 181110A: Enhanced Swift-XRT Position*; GRB Coordinates Network, Circular Service, No. 23417, #1; NASA: Washington, DC, USA, 2018.
19. Kuin, N.P.M.; Evans, P.A. *GRB 181110A: Swift/UVOT Detection*; GRB Coordinates Network, Circular Service, No. 23419, #1; NASA: Washington, DC, USA, 2018.

20. Perley, D.A.; Malesani, D.B.; Fynbo, J.P.U.; Heintz, K.E.; Kann, D.A.; D'Elia, V.; Izzo, L.; Tanvir, N.R. *GRB 181110A: VLT/X-Shooter Redshift*; GRB Coordinates Network, Circular Service, No. 23421, #1; NASA: Washington, DC, USA, 2018.
21. Beuermann, K.; Hessman, F.V.; Reinsch, K.; Nicklas, H.; Vreeswijk, P.M.; Galama, T.J.; Rol, E.; Van Paradijs, J.; Kouveliotou, C.; Frontera, F.; et al. VLT observations of GRB 990510 and its environment. *Astron. Astrophys.* **1999**, *352*, L26–L30.
22. Kann, D.A.; Schady, P.; Olivares, E.F.; Klose, S.; Rossi, A.; Perley, D.A.; Zhang, B.; Kruhler, T.; Greiner, J.; Guelbenzu, A.N.; et al. The optical/NIR afterglow of GRB 111209A: Complex yet not unprecedented. *Astron. Astrophys.* **2018**, *617*, A122. [CrossRef]
23. Foreman-Mackey, D.; Hogg, D.W.; Lang, D.; Goodman, J. emcee: The MCMC Hammer. *Publ. Astron. Soc. Pac.* **2013**, *125*, 306. [CrossRef]
24. Scargle, J.D.; Norris, J.P.; Jackson, B.; Chiang, J. Studies in Astronomical Time Series Analysis. VI. Bayesian Block Representations. *Astrophys. J.* **2013**, *764*, 167. [CrossRef]
25. Schlafly, E.F.; Finkbeiner, D.P. Measuring Reddening with Sloan Digital Sky Survey Stellar Spectra and Recalibrating SFD. *Astrophys. J.* **2011**, *737*, 103. [CrossRef]
26. Evans, P.A.; Beardmore, A.P.; Page, K.L.; Osborne, J.P.; O'Brien, P.T.; Willingale, R.; Starling, R.L.C.; Burrows, D.N.; Godet, O.; Vetere, L.; et al. Methods and results of an automatic analysis of a complete sample of Swift-XRT observations of GRBs. *Mon. Not. R. Astron. Soc.* **2009**, *397*, 1177–1201. [CrossRef]
27. Fitzpatrick, E.L.; Massa, D. An Analysis of the Shapes of Ultraviolet Extinction Curves. III. an Atlas of Ultraviolet Extinction Curves. *Astrophys. J. Suppl. Ser.* **1990**, *72*, 163. [CrossRef]
28. Gordon, K.D.; Clayton, G.C.; Misselt, K.A.; Landolt, A.U. A Quantitative Comparison of the Small Magellanic Cloud, Large Magellanic Cloud, and Milky Way Ultraviolet to Near-Infrared Extinction Curves. *Astrophys. J.* **2003**, *594*, 279–293. [CrossRef]
29. Li, A.; Liang, S.L.; Kann, D.A.; Wei, D.M.; Klose, S.; Wang, Y.J. On Dust Extinction of Gamma-Ray Burst Host Galaxies. *Astrophys. J.* **2008**, *685*, 1046–1051. [CrossRef]
30. Evans, P.A.; Page, K.L.; Sakamoto, T. The Swift Burst Analyser. I. BAT and XRT spectral and flux evolution of gamma ray bursts. *Astron. Astrophys.* **2010**, *519*, A102. [CrossRef]
31. Ryan, G.; Van Eerten, H.; Piro, L.; Troja, E. Gamma-ray burst afterglows in the multimessenger era: Numerical models and closure relations. *Astrophys. J.* **2020**, *896*, 166. [CrossRef]
32. Mészáros, P.; Rees, M.J.; Wijers, R.A.M.J. Viewing Angle and Environment Effects in Gamma-Ray Bursts: Sources of Afterglow Diversity. *Astrophys. J.* **1998**, *499*, 301. [CrossRef]
33. Dai, Z.G.; Gou, L.J. Gamma-Ray Burst Afterglows from Anisotropic Jets. *Astrophys. J.* **2001**, *552*, 72–80. [CrossRef]
34. Rossi, E.; Lazzati, D.; Rees, M.J. Afterglow light curves, viewing angle and the jet structure of γ-ray bursts. *Mon. Not. R. Astron. Soc.* **2002**, *332*, 945–950. [CrossRef]
35. Zhang, B.; Mészáros, P. Gamma-Ray Burst Beaming: A Universal Configuration with a Standard Energy Reservoir? *Astrophys. J.* **2002**, *571*, 876–879. [CrossRef]
36. Kumar, P.; Granot, J. The Evolution of a Structured Relativistic Jet and Gamma-Ray Burst Afterglow Light Curves. *Astrophys. J.* **2003**, *591*, 1075–1085. [CrossRef]
37. Gao, H.; Lei, W.H.; Zou, Y.C.; Wu, X.F.; Zhang, B. A complete reference of the analytical synchrotron external shock models of gamma-ray bursts. *New Astron. Rev.* **2013**, *57*, 141–190. [CrossRef]
38. Jin, Z.P.; Fan, Y.Z. GRB 060418 and 060607A: The medium surrounding the progenitor and the weak reverse shock emission. *Mon. Not. R. Astron. Soc.* **2007**, *378*, 1043–1048. [CrossRef]
39. Sari, R. Hydrodynamics of Gamma-Ray Burst Afterglow. *Astrophys. J.* **1997**, *489*, L37–L40. [CrossRef]
40. Mészáros, P. Gamma-ray bursts. *Rep. Prog. Phys.* **2006**, *69*, 2259–2321. [CrossRef]
41. Racusin, J.L.; Oates, S.R.; Schady, P.; Burrows, D.N.; De Pasquale, M.; Donato, D.; Gehrels, N.; Koch, S.; McEnery, J.; Piran, T.; et al. Fermi and Swift Gamma-ray Burst Afterglow Population Studies. *Astrophys. J.* **2011**, *738*, 138. [CrossRef]
42. Liang, E.W.; Li, L.; Gao, H.; Zhang, B.; Liang, Y.F.; Wu, X.F.; Yi, S.X.; Dai, Z.G.; Tang, Q.W.; Chen, J.M.; et al. Comprehensive Study of Gamma-Ray Burst Optical Emission. II. Afterglow Onset and Late Re-brightening Components. *Astrophys. J.* **2013**, *774*, 13. [CrossRef]
43. Liang, E.W.; Lin, T.T.; Lü, J.; Lu, R.J.; Zhang, J.; Zhang, B. A Tight L_{iso}-$E_{p,z}$-$Gamma_0$ Correlation of Gamma-Ray Bursts. *Astrophys. J.* **2015**, *813*, 116. [CrossRef]
44. Amati, L.; Frontera, F.; Tavani, M.; Antonelli, A.; Costa, E.; Feroci, M.; Guidorzi, C.; Heise, J.; Masetti, N.; Montanari, E.; et al. Intrinsic spectra and energetics of BeppoSAX Gamma-Ray Bursts with known redshifts. *Astron. Astrophys.* **2002**, *390*, 81–89. [CrossRef]
45. Zhang, B.; Zhang, B.B.; Virgili, F.J.; Liang, E.W.; Kann, D.A.; Wu, X.F.; Proga, D.; Lv, H.J.; Toma, K.; Meszaros, P.; et al. Discerning the Physical Origins of Cosmological Gamma-ray Bursts Based on Multiple Observational Criteria: The Cases of z = 6.7 GRB 080913, z = 8.2 GRB 090423, and Some Short/Hard GRBs. *Astrophys. J.* **2009**, *703*, 1696–1724. [CrossRef]
46. Zhang, B.B.; Zhang, B.; Sun, H.; Lei, W.H.; Gao, H.; Li, Y.; Shao, L.; Zhao, Y.; Hu, Y.D.; L.ü; H.J.; et al. A peculiar low-luminosity short gamma-ray burst from a double neutron star merger progenitor. *Nat. Commun.* **2018**, *9*, 447. [CrossRef]